



ELSEVIER

Journal of Computational and Applied Mathematics 109 (1999) 231–242

JOURNAL OF
COMPUTATIONAL AND
APPLIED MATHEMATICS

www.elsevier.nl/locate/cam

The viscous gas ring as an astrophysical test problem for a viscous SPH-code

R. Speith*, H. Riffert

*Institut für Astronomie und Astrophysik, Universität Tübingen, Auf der Morgenstelle 10,
D-72076 Tübingen, Germany*

Received 18 January 1999; received in revised form 20 April 1999

Abstract

We present the general analytic solution of a viscous gas ring around a central mass. This solution is used to test a further development of the smoothed particle hydrodynamics (SPH) algorithm, which is capable of simulating problems with physical viscosity (here: with kinematic viscosity). We discuss some SPH simulation results and conclude some fundamental properties of the algorithm. © 1999 Elsevier Science B.V. All rights reserved.

Keywords: Numerical hydrodynamics; Particle methods; SPH benchmark problem

1. Introduction

A large class of problems in theoretical astrophysics is related to the dynamics of compressible flows including many physical effects such as gravity, radiation, viscosity, electric charges and currents, or magnetic fields. These problems are attacked primarily through numerical simulations, and different numerical methods for various aspects of astrophysical gas dynamics have been developed in the past or are currently in the state of development. These algorithms have to be tested in order to verify their stability, accuracy, and robustness. An ideal test is, of course, a comparison with a model problem where an analytic solution is known, and examples for one-dimensional flows include the well-known shock tube, advection problems (see the article of Stone [14] in this volume), or self-similar solutions of the Euler equation for a perfect gas. For many numerical methods error estimates are impossible to obtain, and analytic solutions can be used to determine error bounds empirically. This is even more important when the mathematical foundations of the method are poorly understood, and one such method is smoothed particle hydrodynamics (SPH). For two- or

* Corresponding author.

E-mail address: speith@tat.physik.uni-tuebingen.de (R. Speith)

three-dimensional gas flows analytically solvable problems are rare but there is one astrophysically interesting example where at least an approximate solution of the hydrodynamic equations can be found. This is concerned with a thin gas disk that moves around a central point mass under the influence of gravity and viscous torques. If rotational symmetry is assumed an evolution equation for the density can be derived, and for a constant kinematic viscosity the solution of an initial value problem is obtained explicitly in terms of Bessel functions and exponentials [7,10,2].

The purpose of this paper is to use the above analytic solution as a test model for a SPH code that is designed to simulate two-dimensional viscous gas flows dominated by gravitational forces. The analytic solution is briefly discussed in Section 2 for the case that the viscosity varies as a power of the radial coordinate. In Section 3, the SPH method is introduced with special emphasis on the implementation of the physical viscosity. The actual numerical tests are presented in Section 4.

2. The viscous gas ring

We consider an axisymmetric thin disk of gas moving around a central point mass M_c under the influence of gravity and viscous stresses. For such a flow we can define two small quantities. First, the height H of the disk is assumed to be negligible compared to the radial length scale, and secondly, the viscous time scale of the radial inflow of mass is much smaller than the dynamical time scale of a circular orbit. As a consequence of the thin-disk approximation, it is possible to integrate the dynamic equations over the height of the disk. The resulting flow structure is now two-dimensional, note however that this flow is embedded in \mathbb{R}^3 , and therefore the gravitational force is still proportional to r^{-2} . Polar coordinates (R, φ) are used, there are only two velocity components (v_R, v_φ) , and the mass distribution is described in terms of the surface density

$$\Sigma(R, t) = \int_{-H}^{+H} \rho \, dz,$$

where ρ is the mass density. With these assumption the equation of continuity reads

$$\frac{\partial \Sigma}{\partial t} + \frac{1}{R} \frac{\partial (R \Sigma v_R)}{\partial R} = 0, \tag{1}$$

whereas the R - and φ -component of the Navier–Stokes equation are given by

$$\begin{aligned} \frac{\partial v_R}{\partial t} + v_R \frac{\partial v_R}{\partial R} - \frac{v_\varphi^2}{R} = & -\frac{GM_c}{R^2} + \frac{1}{\Sigma} \frac{2}{R} \left(\frac{\partial}{\partial R} \left[v_s \Sigma \left(\frac{2}{3} \frac{\partial (R v_R)}{\partial R} - v_R \right) \right] \right. \\ & \left. + \frac{v_s \Sigma}{R} \left(\frac{1}{3} \frac{\partial (R v_R)}{\partial R} - v_R \right) \right), \end{aligned} \tag{2}$$

$$\frac{\partial v_\varphi}{\partial t} + v_R \frac{\partial v_\varphi}{\partial R} + \frac{v_R v_\varphi}{R} = \frac{1}{\Sigma} \frac{1}{R^2} \frac{\partial}{\partial R} \left[R^3 v_s \Sigma \frac{\partial}{\partial R} \left(\frac{v_\varphi}{R} \right) \right]. \tag{3}$$

Here, v_s is the kinematic viscosity and G is the gravitational constant, and radial pressure forces are neglected. These equations are considered in the limit of a small viscosity, i.e., it is assumed that the radial inflow of mass is caused entirely by viscous stresses. Thus, v_R is small ($v_R \ll v_\varphi$) and vanishes in the limit $v_s \rightarrow 0$. Taking $v_s = 0$, i.e., $v_R = 0$, Eq. (2) reduces to its dominant terms

$$-\frac{v_\varphi^2}{R} = -\frac{GM_c}{R^2} \tag{4}$$

which indicates that the gas moves essentially with Kepler velocity

$$v_\phi = \sqrt{\frac{GM_c}{R}} \tag{5}$$

around the central mass. Using the expression (5) in (3) we obtain

$$R\Sigma v_R = -3\sqrt{R} \frac{\partial}{\partial R} (v_s \sqrt{R}\Sigma) \tag{6}$$

which shows that v_R is in fact $O(v_s)$. Eq. (6) together with the continuity equation (1) leads to a parabolic evolution equation for the surface density

$$\frac{\partial \Sigma}{\partial t} = \frac{3}{R} \frac{\partial}{\partial R} \left[\sqrt{R} \frac{\partial}{\partial R} (v_s \sqrt{R}\Sigma) \right]. \tag{7}$$

An analytic solution can be obtained on the space domain $[0, \infty)$ with initial data

$$\Sigma(R, 0) = \Sigma_0(R)$$

provided the kinematic viscosity has the form

$$v_s(R) = v_0 R^\gamma, \tag{8}$$

where v_0 and γ are constants. According to the standard thin-disk theory [10,2] the disk is likely to be in a state of fully excited turbulence and v_s is interpreted as a turbulent viscosity. Therefore, v_s will in general depend on the radius and the particular form (8) has been chosen in order to keep the problem analytically solvable.

For $\gamma = 0$ the solution of (7) is given, for example, by Pringle [10] or Frank et al. [2]. A more general solution has been calculated by Lüst [7]. There are two possible branches of the solution: either the mass can be conserved, then the angular momentum of the system is not and has a source or drain at the origin. Or the angular momentum of the system is conserved and the mass of the disk has a drain at the origin. The latter is a representation of an accretion disk.

If the initial density distribution is chosen to be an infinitesimal ring of mass M at an initial radius R_0 we have for Σ_0

$$\Sigma_0(R) = \frac{M}{2\pi R_0} \delta(R - R_0) \tag{9}$$

and the surface density reads

$$\Sigma(R, t) = \frac{M}{\pi R_0^2} \left(1 - \frac{\gamma}{2}\right) \frac{1}{\tau x^{1/4+\gamma}} I_n \left(\frac{2x}{\tau x^{\gamma/2}}\right) \exp\left(-\frac{1+x^{2-\gamma}}{\tau}\right) \tag{10}$$

with

$$n := \frac{1}{4 - 2\gamma}, \quad x := \frac{R}{R_0}, \quad \tau := \frac{12v_0 t}{R_0^{2-\gamma}} \quad (\gamma < 2).$$

Here I_n is the modified Bessel function of order n , and the dimensionless variable τ is the time in units of the viscous time scale $R_0^{2-\gamma}/(12v_0)$.

With the surface density (10) the radial velocity v_R becomes

$$v_R = \frac{3(2 - \gamma)v_0 R_0^{\gamma-1}}{\tau} \left[x - x^{\gamma/2} I_{n-1} \left(\frac{2x}{\tau x^{\gamma/2}}\right) \right] / I_n \left(\frac{2x}{\tau x^{\gamma/2}}\right). \tag{11}$$

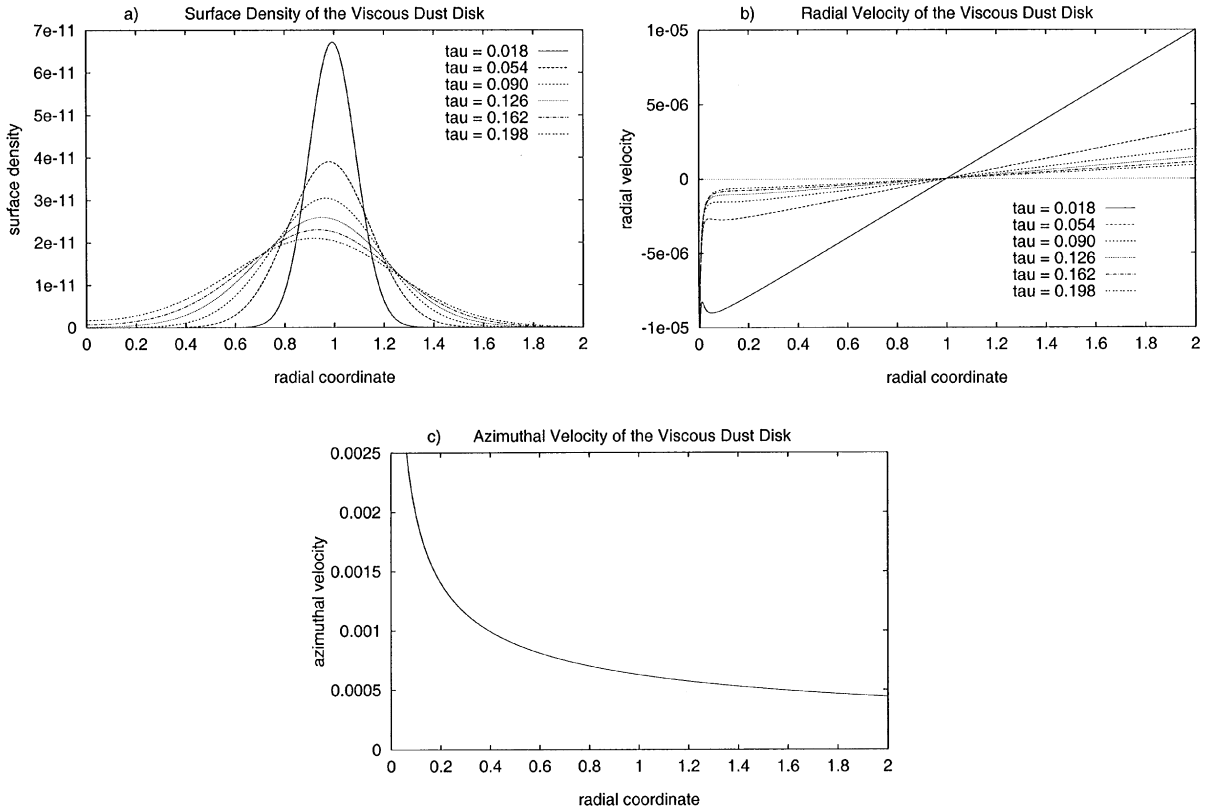


Fig. 1. Analytic solution of the viscous gas ring with $\gamma=0$, initial radius $R_0=1R_\odot$, kinematic viscosity $\nu_0=1.5 \times 10^{14} \text{ cm}^2/\text{s}$, disk mass $M = 10^{-10} M_\odot$, and central mass $M_c = 1 M_\odot$. Plotted are: (a) the surface density Σ , (b) the radial velocity v_R , and (c) the azimuthal velocity v_ϕ at different viscous times τ .

Eqs (5), (10), and (11) are used to calculate the reference solution for our numerical simulation in Section 4.

In Fig. 1, the evolution of the ring is shown for the case $\gamma = 0$, i.e. $v_s = v_0 = \text{const}$. Comparing the radial velocity at various viscous times in Fig. 1(b) with the Keplerian velocity in Fig. 1(c) shows that the approximation $v_R \ll v_\phi$ is always justified. Note that the parameters given in Fig. 1 have been used throughout the simulations presented in Section 4.

3. Viscous SPH

The SPH method was introduced 1977 by Gingold and Monaghan [3] and Lucy [6] to simulate compressible flows with free boundaries. For an overview of the SPH method see, for example, [8]. The article of Rasio and Lombardi [11] in this volume gives also a short introduction into the basics of SPH.

In the standard SPH codes, viscosity is usually implemented only through an artificial viscous pressure term which is necessary to handle shock fronts correctly [9]. This artificial viscosity,

however, is not a proper description of the viscous processes associated with the shear or bulk viscosity of real fluids. For this reason, we have included in our SPH algorithm the entire viscous stress tensor according to the Navier–Stokes equation [1]. This implementation allows for the proper treatment of viscous shear flows. In Lagrangian formulation, the viscous part of the Navier–Stokes equation reads

$$\left. \frac{dv_\alpha}{dt} \right|_{\text{visc.}} = \frac{1}{\rho} \frac{\partial T_{\alpha\beta}}{\partial x_\beta} \tag{12}$$

with (volume) density ρ and the viscous stress tensor

$$T_{\alpha\beta} = \rho v \left(\frac{\partial v_\alpha}{\partial x_\beta} + \frac{\partial v_\beta}{\partial x_\alpha} - \frac{2}{3} \delta_{\alpha\beta} \frac{\partial v_\gamma}{\partial x_\gamma} \right) + \zeta \delta_{\alpha\beta} \frac{\partial v_\gamma}{\partial x_\gamma}. \tag{13}$$

Here x_α denotes Cartesian coordinates and Greek indices take the values 1, 2, 3; in addition Einstein’s summing convention is assumed for the coordinates. The coefficients v and ζ , i.e., the kinematic shear and the bulk viscosity, are positive scalars and are independent of the velocity. Although the treatment of bulk viscosity is no principal problem we use $\zeta = 0$ throughout.

Applying the smoothing discretization scheme to the derivative of the stress tensor yields the SPH representation

$$\left. \frac{dv_{\alpha i}}{dt} \right|_{\text{visc.}} = \sum_j \frac{m_j}{\rho_i \rho_j} (T_{\alpha\beta i} + T_{\alpha\beta j}) \frac{\partial}{\partial x_{\beta i}} W(|\mathbf{r}_i - \mathbf{r}_j|; h) \tag{14}$$

with the particle form of the stress tensor

$$T_{\alpha\beta i} = \rho_i v_i (V_{\alpha\beta i} + V_{\beta\alpha i} - (\frac{2}{3}) \delta_{\alpha\beta} V_{\gamma\gamma i}), \tag{15}$$

where $V_{\alpha\beta i}$ is the particle representation of the velocity gradient $\partial v_\alpha / \partial x_\beta$

$$V_{\alpha\beta i} = \frac{\partial v_{\alpha i}}{\partial x_{\beta i}} = \sum_j \frac{m_j}{\rho_j} (v_{\alpha j} - v_{\alpha i}) \frac{\partial}{\partial x_\beta} W(|\mathbf{r}_i - \mathbf{r}_j|; h). \tag{16}$$

The indices i and j denote quantities that are assigned to SPH particles with positions \mathbf{r}_i and \mathbf{r}_j , respectively; m_j is the particle mass, and W is the SPH kernel function. The kernel W depends on the distance between particles i and j and on the smoothing length h , which is a measure of the support of the kernel.

One advantage of this treatment of viscosity is that the shear and the bulk viscosity can be specified explicitly and independently, which is not the case for the usual artificial viscosity terms. On the other hand, this method leads to a significant increase of CPU time and computer memory. Since (14) together with (16) contains double sums over all N_p SPH particles one has to be careful not to construct N^2 - or N^3 -algorithms. This can be avoided, for example, by summing over interaction pairs instead of single particles.

For a more detailed description of our method and for questions concerning energy balance, linear and angular momentum conservation we refer to Riffert et al. [12] or Speith [13]. All other SPH equations are formulated in our code more or less in the standard way, their representation can be found elsewhere, for example, in [8] or [11].

4. SPH simulations of the viscous ring

We have performed various simulations of the gas ring described in Section 2 using the viscous SPH scheme discussed in the previous section. As an example, we present simulations with a constant viscosity (i.e., $\gamma = 0$), initial radius $R_0 = 1R_\odot$, disk mass $M = 10^{-10}M_\odot$, and central mass $M_c = 1M_\odot$. Here $R_\odot = 7 \times 10^{10}$ cm is the solar radius, and $M_\odot = 2 \times 10^{33}$ g denotes the solar mass. For the kinematic viscosity we take $\nu_0 = 1.5 \times 10^{14}$ cm²/s which is approximately equal to or a little less than the value of the turbulent viscosity in a typical astrophysical accretion disk in a binary star system (see [5]).

According to (9), the density distribution at viscous time $\tau = 0$ is a δ -function, thus we take $\tau = 0.018$ as the starting time for our simulations. Consequently, the initial SPH particle distributions have to be created in such a way that they represent the analytic density (10) at $\tau = 0.018$, and every particle moves with an initial velocity according to (5) and (11). Fig. 2 shows the SPH particle positions for three differently generated initial distributions. The left column corresponds to the initial time $\tau = 0.018$, and the right column shows the simulations at $\tau = 0.126$.

In Fig. 2(a.1) the particle positions are equally spaced on concentric rings around the origin. During the simulation this uniform particle distribution is destroyed (see Fig. 2(a.2)). Since the particles move essentially on Keplerian orbits, there is a strong difference in the azimuthal velocity of neighbouring orbits, and thus even small radial velocities lead to a fast de-correlation of the particle positions. However, a certain amount of correlation is preserved as the flow evolves in time. This is visible as a system of concentric rings in the particle distribution (Fig. 2(a.2)), but the details of this process are not fully understood yet.

These structures disappear if the particles are distributed initially in a stochastic way, i.e., the positions are randomly chosen according to a probability density that corresponds to the initial surface density $\Sigma(R, t = t_0)$ (see Fig. 2(b.1) and (b.2)). The initial distribution in Fig. 2(b.1) has a point symmetry with respect to the origin which guarantees that the centre of mass is located at $R = 0$. This initial symmetry is violated in the example shown in Fig. 2(c.1), and, as a result, spiral structures appear in the particle distribution. The same spirals will also show up for the point-symmetric initial conditions of Fig. 2(b.1) but at much later times. This could indicate that the entire flow is unstable with respect to nonaxisymmetric perturbations, and that the initial amplitude of those perturbations is strongly reduced if the particle positions are set up with an initial point symmetry. It is, however, not clear what the nature of this instability is, i.e., whether it is purely numerical in origin or has a physical cause such as a viscous over-stability (cf. [4]).

To further investigate the properties of the SPH method we will now focus our attention on the physical quantities rather than analysing the distribution of particle positions. In Fig. 3 we show the surface density Σ computed at viscous time $\tau = 0.126$ of a SPH simulation with the initial particle distribution from Fig. 2(b.1), i.e. with $N_p = 10\,000$ particles, and a smoothing length of $h = 0.09R_\odot$.

Fig. 3(a) shows the values of the surface density for each SPH particle projected onto the radial coordinate. Note the large fluctuations of the results around the analytic solution (indicated by the dashed line). Because of this large scattering, an averaging of the results is necessary for further evaluations.

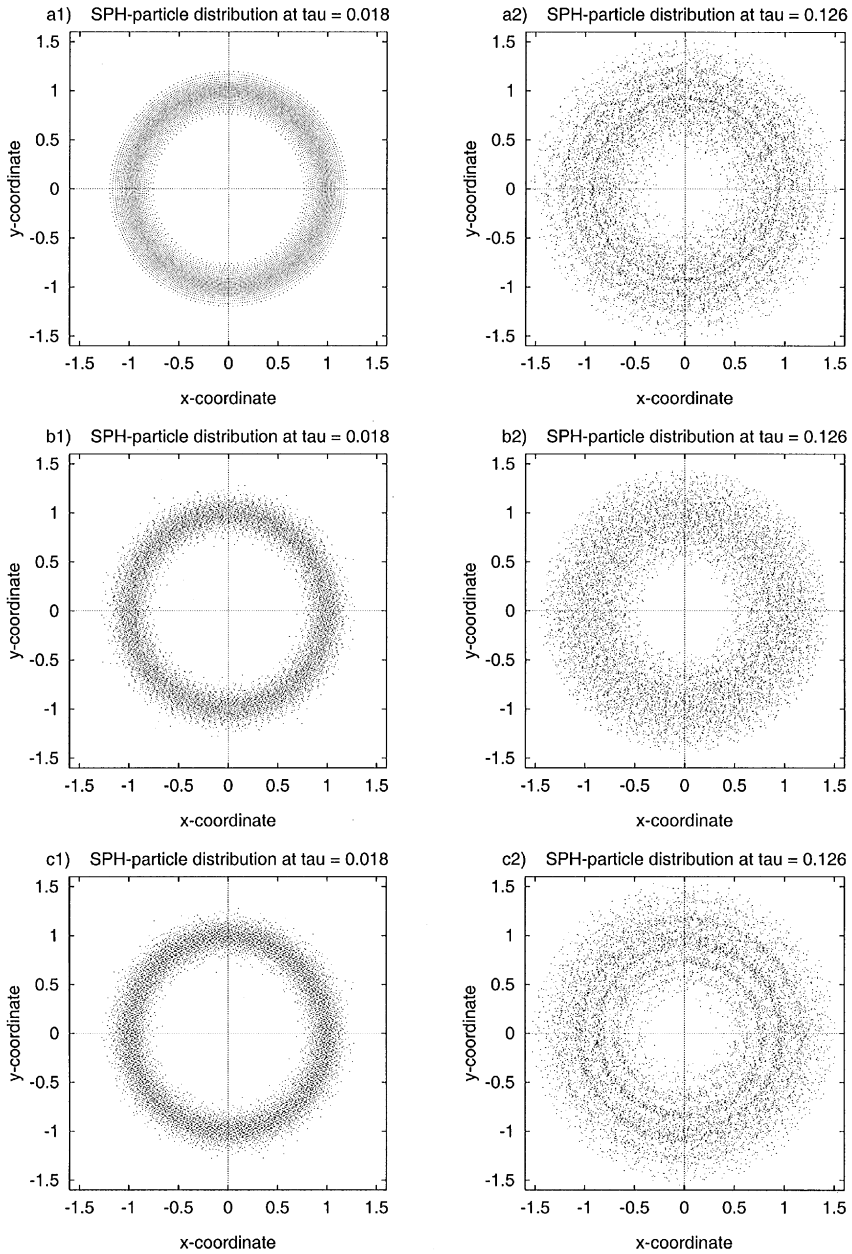


Fig. 2. Simulation results for different initial SPH particle distributions. (a) Initial particles equally spaced on concentric rings around $R=0$. (b) Random initial distribution but point symmetric with respect to $R=0$. (c) Random initial distribution without point symmetry. Left column: particle distribution at the initial time $\tau = 0.018$. Right column: distribution at $\tau = 0.126$.

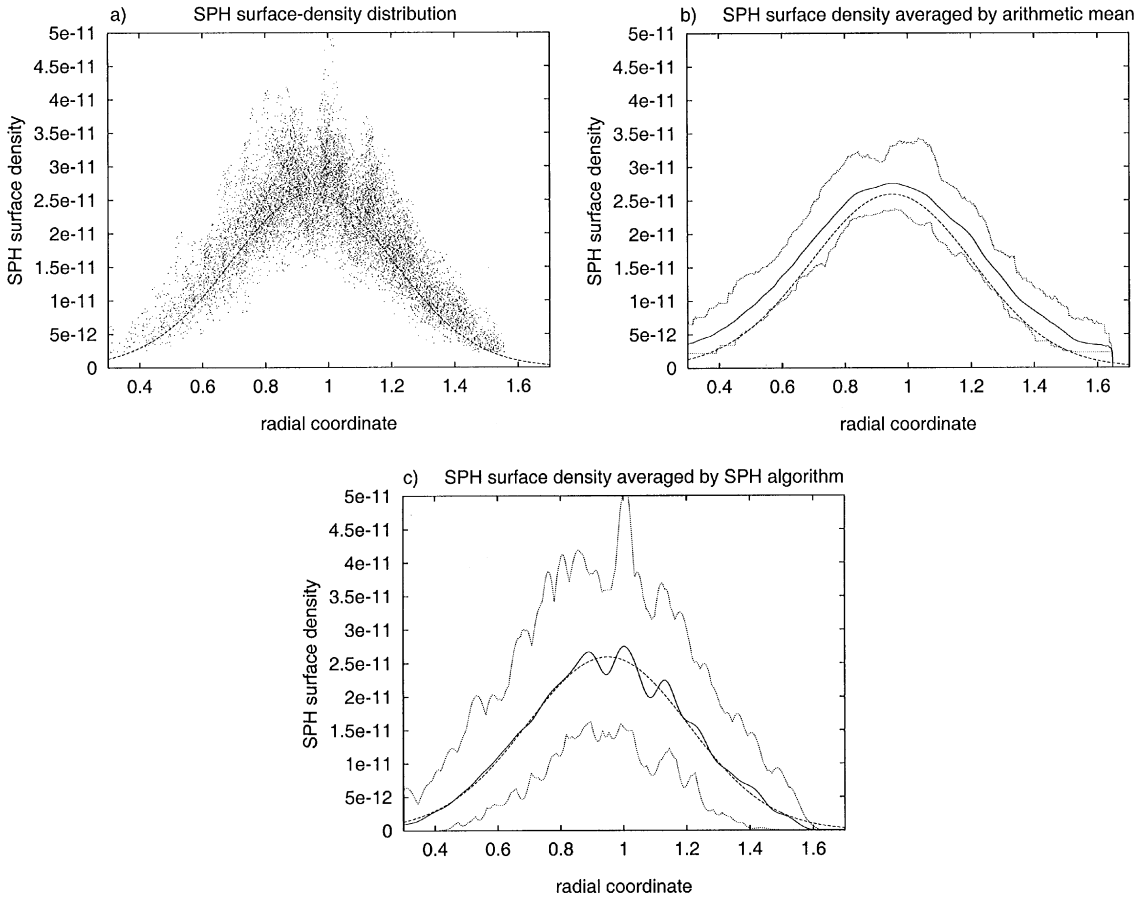


Fig. 3. Different ways to evaluate the density from the simulation results (here: $h = 0.09R_{\odot}$, $N_p = 10\,000$). (a) Distribution of density values Σ at particle positions. (b) Density $\bar{\Sigma}$ averaged by arithmetic mean. (c) Density $\bar{\Sigma}$ averaged by SPH algorithm. Dotted: upper and lower limits $\bar{\Sigma}_{\max}$ and $\bar{\Sigma}_{\min}$ of the azimuthal averaged values. Dashed: analytic solution.

One possibility of averaging is using an arithmetic mean

$$\Sigma_{\text{eval}}(\mathbf{r}) = \frac{1}{N_h} \sum_j \Sigma(\mathbf{r}_j) \quad \text{with } j \in \{\text{particles with } |\mathbf{r} - \mathbf{r}_j| \leq h\}, \tag{17}$$

where \mathbf{r} is an arbitrary position in space and N_h is the number of SPH particles which can interact with position \mathbf{r} , i.e., for which $|\mathbf{r} - \mathbf{r}_j| \leq h$ holds. After that, the surface density Σ_{eval} is additionally averaged over the azimuthal angle

$$\bar{\Sigma}(R) = \frac{1}{N_a} \sum_{l=1}^{N_a} \Sigma_{\text{eval}}(\mathbf{r}_l^{N_a}) \quad \text{with } |\mathbf{r}_l^{N_a}| = R. \tag{18}$$

Here, a number of N_a equally spaced positions \mathbf{r}^{N_a} on the circle with radius R have to be chosen. In addition, we calculate upper and lower bounds

$$\bar{\Sigma}_{\max}(R) = \max_{l=1 \dots N_a} [\Sigma_{\text{eval}}(\mathbf{r}_l^{N_a})], \quad \bar{\Sigma}_{\min}(R) = \min_{l=1 \dots N_a} [\Sigma_{\text{eval}}(\mathbf{r}_l^{N_a})]. \tag{19}$$

Fig. 3(b) presents the results of the simulation averaged in this way. The straight line indicates the average density $\bar{\Sigma}$, and the upper and lower lines show the values of $\bar{\Sigma}_{\max}$ and $\bar{\Sigma}_{\min}$, respectively. It can be seen clearly that $\bar{\Sigma}$ matches the shape of the analytic solution (dashed line) quite accurately, but lies always a certain amount above that solution. This overestimation of the true density by the SPH density is a selection effect due to the stochastic nature of this special particle distribution, combined with the usual way to calculate the SPH density

$$\Sigma_i = \sum_j m_j W(|\mathbf{r}_i - \mathbf{r}_j|; h)$$

(for a detailed explanation see [15]). In a SPH simulation with dominant hydrodynamic forces such as pressure or viscous shear, the particles tend to establish a correlation which reduces the stochastic nature of the initial distribution, and no overestimation of the density occurs. But for the problem of the viscous ring, the differential rotation, caused by the strong gravitational forces, prevents and destroys every correlation developing between the SPH particles.

The selection effect occurs if the density is considered exclusively at the particle positions as is the case in the averaging process defined in (17). The overestimation problem can be avoided if the density is computed according to the SPH algorithm but at arbitrary positions \mathbf{r} and not necessarily at particle positions \mathbf{r}_j , i.e.,

$$\Sigma_{\text{eval}}(\mathbf{r}) = \sum_j m_j W(|\mathbf{r} - \mathbf{r}_j|; h), \quad j \in \{\text{particles with } |\mathbf{r} - \mathbf{r}_j| \leq h\}. \quad (20)$$

(Besides, averaging by (20) emphasises the continuum-picture of the SPH method). In Fig. 3(c) the straight line indicates the surface density $\bar{\Sigma}$ according to (20) after an additional azimuthal averaging according to (18). The simulated and averaged density fits the analytic solution (dashed line) quite well. The density is no longer systematically overestimated, although now a wave-like fluctuation appears in the average density indicating an underlying ring or narrow spiral structure. The upper and lower lines again represent the bounds $\bar{\Sigma}_{\max}$ and $\bar{\Sigma}_{\min}$ calculated from (19). Furthermore, comparing Fig. 3(c) and (a) confirms that these upper and lower bounds are reasonable measures for the range of fluctuations of the SPH results.

The large scattering of the SPH results indicates the stochastic nature of the particle distribution as well. This can be concluded from Fig. 4, where the results of SPH simulations are shown which have identical initial conditions but use different values for the numerical parameters. In Fig. 4(a) and (b) the particle number N_p is 10 000, whereas in Fig. 4(c) and (d) 40 000 particles were used. Nevertheless, the results shown in Fig. 4(a) and (c) are quite similar including the range of fluctuations of the surface density. The same is true for the simulations shown in Fig. 4(b) and (d).

The common property of the cases in Fig. 4(a) and (c) (or Fig. 4(b) and (d), respectively) is that the same mean interaction number N_i is used. The interaction number of a particle i is the number of all those particles j with $|\mathbf{r}_i - \mathbf{r}_j| \leq h$, and we have $N_i \propto h^d N_p$ where d is the dimension of the problem, i.e., $d = 2$ for the viscous ring. Therefore, the mean interaction number remains constant when the particle number N_p is multiplied by four and the smoothing length h is halved, as is done comparing the simulation in Fig. 4(a) to the one in (c) and the one in Fig. 4(b) to the one in (d), respectively.

Comparing Fig. 4(a) and (b) the smoothing length has been almost doubled keeping N_p constant. Thus the interaction number is nearly four times higher in Fig. 4(b) than in (a). Simultaneously, the range of scattering of the SPH results around the analytic solution is reduced by a factor of about

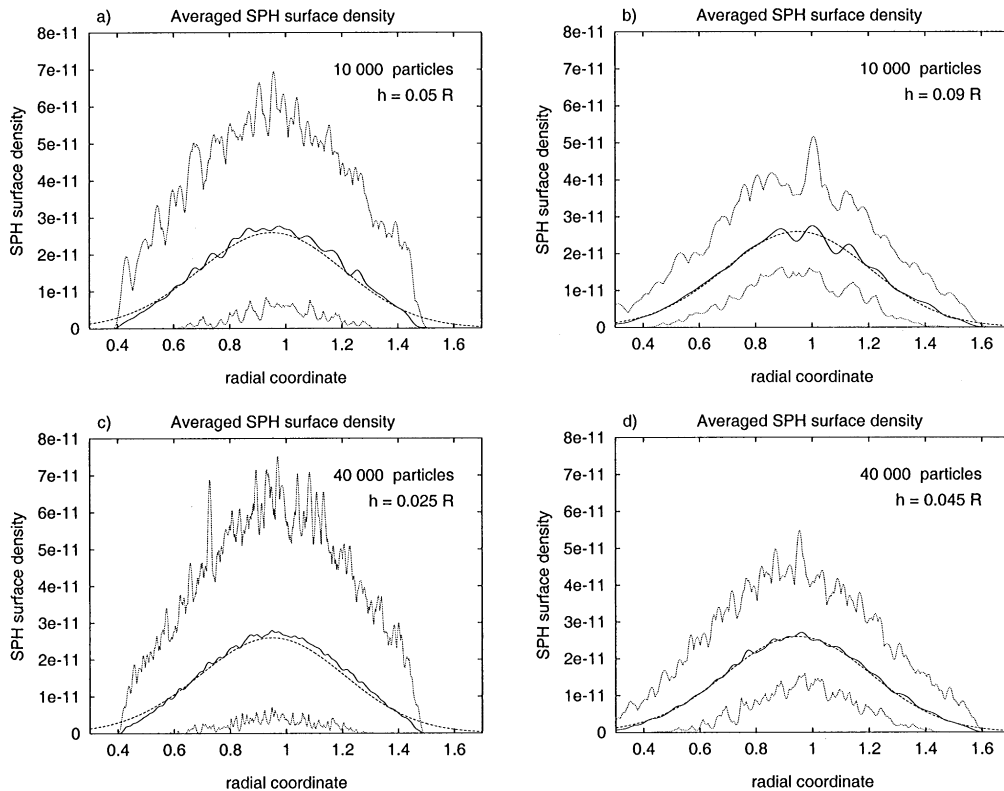


Fig. 4. Comparison of averaged density $\bar{\Sigma}$ (straight line) with upper and lower limit $\bar{\Sigma}_{\max}$ and $\bar{\Sigma}_{\min}$ (dotted) at $\tau = 0.126$ (dashed line) for different particle numbers and smoothing lengths: (a) $N_p = 10\,000$, $h = 0.05R_\odot$, (b) $N_p = 10\,000$, $h = 0.09R_\odot$, (c) $N_p = 40\,000$, $h = 0.025R_\odot$, (d) $N_p = 40\,000$, $h = 0.045R_\odot$.

two. The same holds for the simulation results shown in Fig. 4(c) and (d). This indicates that the fluctuation depends on the interaction number approximately as $1/\sqrt{N_i}$ which shows the stochastic nature of the particle distribution.

Increasing the smoothing length much further for the case in Fig. 4(b) would, however, not improve the result in general, because if the smoothing length is increased, not only the numerical error of the SPH method (which is $O(h^2)$) is increased as well, but the spatial resolution is decreased. This can be seen, for example, in Fig. 4(d) where the averaged surface density matches the analytic solution better than in Fig. 4(b) where the variations around the analytic solution are more prominent.

However, in spite of the large fluctuations discussed above, the SPH simulations are in general able to reproduce the global dynamical behaviour of the viscous gas ring very well. This can be seen in Fig. 5, where the time evolution of the averaged surface density $\bar{\Sigma}$ is presented at several viscous times. From one diagram to the next, a particle at the radius $R = R_0 = 1R_\odot$ circles the central mass approximately 10 times. The ring spreads considerably, but the averaged surface density matches the entire analytic solution quite well at every time step. The remaining deviations could be reduced using a larger mean interaction number N_i (compare Fig. 4(d)).

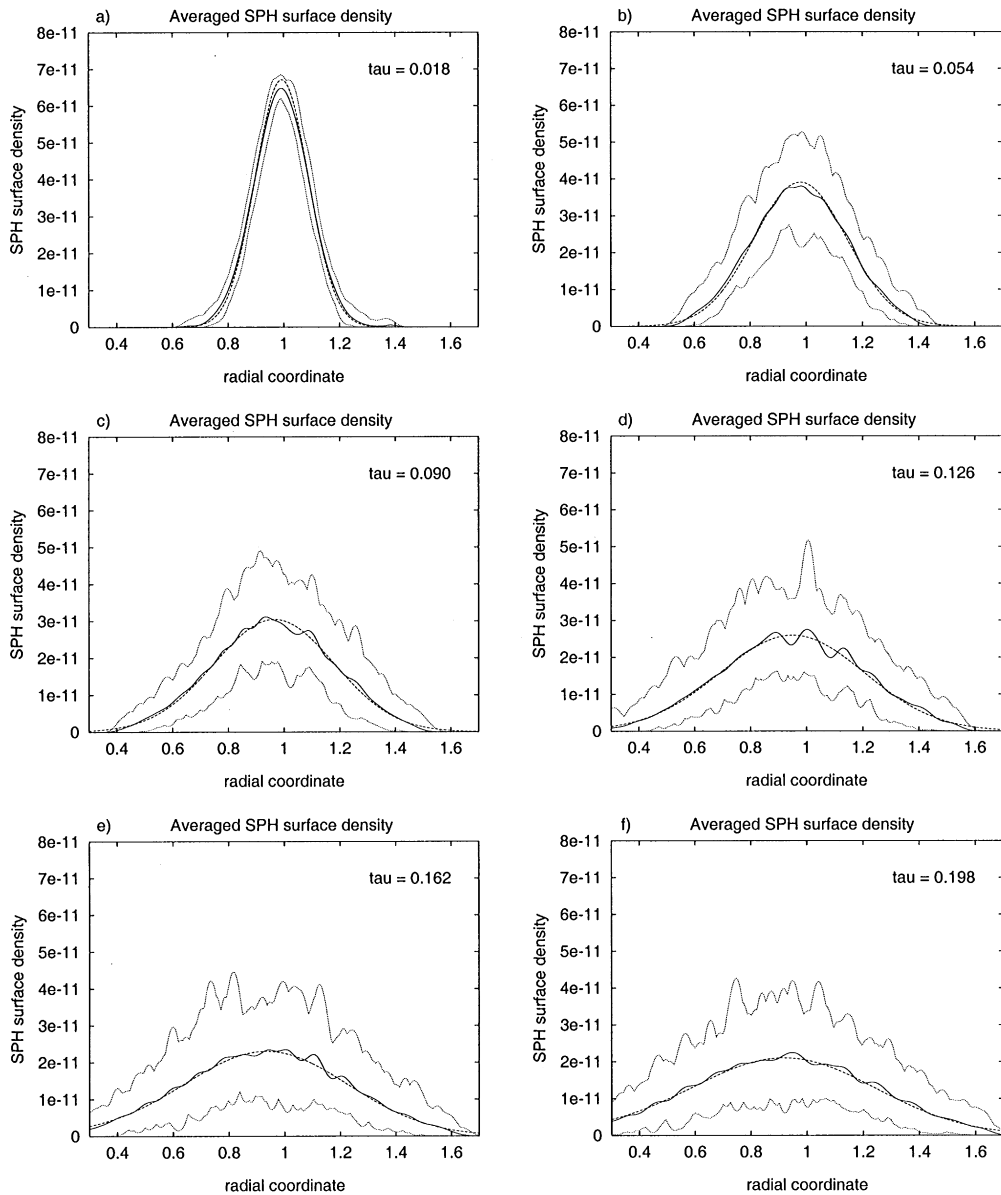


Fig. 5. Evolution of the surface density of the viscous gas ring. Simulation with particle number $N_p = 10\,000$ and smoothing length $h = 0.09R_\odot$. Straight lines: averaged simulation results, dashed lines: analytic solution, dotted lines: range of scattering of the SPH results.

5. Conclusion

The simulations of the viscous gas ring with our viscous SPH have illustrated some important and universal features of this numerical method. One result is, that SPH can in general reproduce global attributes and the dynamical evolution of the considered physical problems. However, the local

accuracy and the spatial resolution of SPH simulations are rather poor. Actually, the results obtained from a two-dimensional SPH code using 10^4 particles should be compared to a finite-difference simulation on a grid of 100×100 cells. Moreover, the SPH results show a large fluctuation of the results, at least if the particle distribution remains in a “stochastic” state, which is always the case when external forces dominate the hydrodynamical forces.

Two fundamental parameters of the method can be identified. The smoothing length h determines the spatial resolution of the simulations, whereas the global accuracy depends on the mean interaction number N_i . The higher N_i and the lower h the better are the simulation results. Because these conditions are partly contradictory, one has to find a compromise by choosing the total particle number N_p according to the computer resources available. In Section 4, only simulations with fixed smoothing lengths are presented, but similar results are obtained for SPH simulations with variable smoothing length where the number of interactions for each particle is kept constant.

Another outcome of the simulations is that the viscous gas ring is in fact a suitable test problem for astrophysical hydro codes independent of the numerical method used. Kley [4], for example, has recently simulated the ring using a finite-difference method. However, the stability of the gas ring against nonaxisymmetric perturbations still has to be investigated.

Acknowledgements

The authors want to thank F. Ott, U. Kraus, E. Schnetter, and W. Kley for many fruitful discussions and contributions. This work was supported by the Deutsche Forschungsgemeinschaft (DFG) and is part of the project A1 of the Sonderforschungsbereich SFB 382.

References

- [1] O. Flebbe, S. Münzel, H. Herold, H. Riffert, H. Ruder, Smoothed particle hydrodynamics: physical viscosity and the simulation of accretion disks, *Astrophys. J.* 431 (1994) 754–760.
- [2] J. Frank, A.R. King, D.J. Raine, *Accretion Power in Astrophysics*, Cambridge University Press, Cambridge, 1992.
- [3] R.A. Gingold, J.J. Monaghan, Smoothed particle hydrodynamics: theory and application to nonspherical stars, *Mon. Not. R. Astron. Soc.* 181 (1977) 375–389.
- [4] W. Kley, private communication, 1998.
- [5] S. Kunze, R. Speith, H. Riffert, Reproducing superhumps and γ -shifts of SU UMa stars with SPH simulations, *Mon. Not. Roy. Astron. Soc.* 289 (1997) 889–897.
- [6] L.B. Lucy, A numerical approach to the testing of the fission hypothesis, *Astron. J.* 82 (12) (1977) 1013–1024.
- [7] R. Lüst, Die Entwicklung einer um einen Zentralkörper rotierenden Gasmasse, *Z. Natur.* 7a (1952) 87–98.
- [8] J.J. Monaghan, Smoothed particle hydrodynamics, *Annu. Rev. Astron. Astrophys.* 30 (1992) 543–574.
- [9] J.J. Monaghan, R.A. Gingold, Shock simulations by the particle method SPH, *J. Comput. Phys.* 52 (1983) 374–389.
- [10] J.E. Pringle, Accretion discs in astrophysics, *Ann. Rev. Astron. Astrophys.* 19 (1981) 137–162.
- [11] F.A. Rasio, J.C. Lombardi, Smoothed particle hydrodynamics calculations of stellar interactions, *J. Comput. Appl. Math.* (1999).
- [12] H. Riffert, H. Herold, O. Flebbe, H. Ruder, Numerical aspects of the smoothed particle hydrodynamics method for simulating accretion disks, *Comput. Phys. Comm.* 89 (1995) 1–16.
- [13] R. Speith, *Untersuchung von Smoothed Particle Hydrodynamics anhand astrophysikalischer Beispiele*, Dissertation, Universität Tübingen, 1998.
- [14] J.M. Stone, Some numerical methods for astrophysical gas dynamics, *J. Comput. Appl. Math.* (1999).
- [15] A.P. Whitworth, A.S. Bhattal, J.A. Turner, S.J. Watkins, Estimating density in smoothed particle hydrodynamics, *Astron. Astrophys.* 310 (1995) 929–932.